Low frequency passive seismic interferometry for land data

Sjoerd de Ridder[1] *and Biondo Biondi, Stanford University*

SUMMARY

Seismic interferometry aims to retrieve the Green's function between two receiver stations by correlating measurements of seismic responses at both stations, effectively turning one station into a virtual source. Passive seismic interferometry has mainly focused on retrieving high-frequency (> 10) Hz virtual sources where acquiring data with real sources is undesirable. Thus far, results of passive seismic interferometry have been less than promising, partially due to directionality of the ambient seismic wavefield and poor sampling of the medium by passive seismic sources. More recently, the ambient seismic field at lower frequencies (< 10) Hz has been shown to contain sufficient coherent and omnidirectional seismic energy to yield low-frequency Green's functions containing direct arrivals in a marine environment. Here we report results achieved by low-frequency seismic interferometry on a land dataset recorded at a field in Saudi Arabia. Results suggest that sufficient coherent energy is recorded between 1 Hz and 7 Hz for retrieval of a Rayleigh surface wave. The strength of the ambient seismic field affects the convergence rate of the correlations. The directionality in the ambient seismic field affects the radiation pattern of the virtual sources. Retrieved Rayleigh waves at low frequencies show spatial variation and dispersive behavior. Dispersion curve estimation opens opportunities for reservoir monitoring by background velocity estimation.

INTRODUCTION

Seismic interferometry is a technnique of cross-correlating signals recorded at two stations to retrieve the impulse response (Green's function) between them (Claerbout, 1968; Wapenaar, 2004). Recently, a variety of applications have been developed for active seismic data, such as the virtual source method (Bakulin and Calvert, 2006), redatuming (Schuster et al., 2004; Schuster and Zhou, 2006), and imaging of multiples (Berkhout and Verschuur, 2006). Commonly, active seismic interferometry attempts to reconstruct the high-frequency impulse response of the earth. Passive seismic interferometry for high-frequency reflection imaging has been less successful. Early attempts of Cole (1995), (Artman, 2006, 2007) yielded less than satisfactory results; more recently, Dragonov et al. (2007) retrieved high-frequency reflection events from pre-selected body-wave events. Meanwhile, global seismologists have been successful using seismic interferometry to retrieve Green's functions at much lower frequency. Dellinger (2008) pointed out that conventional arrays record useable energy at low frequencies. Dellinger and Yu (2009), Landes et al. (2009) and Bussat and Kugler (2009) have reported on the use of low-frequency seismic energy recorded in marine environments to image shallow seafloor structures.

An ambient seismic field recorded above a field in Saudi Arabia has previously been studied using novel imaging methods to locate microseismic events (Fu and Luo, 2009) and seismic interferometery to retrieve high frequency events (Xiao et al., 2009). Here we show interferometric retrieval of the Rayleigh surface waves at low frequencies. These surface waves are further studied for potential reservoir monitoring and imaging capabilities. Data availability limits the study to a conventional microtremor dispersion-curve analysis technique (Aki, 1957), which assumes laterally invariant media. However, more generally the retrieved Green's function can be studied and imaged without implicit lateral invariant assumptions.

AMBIENT SEISMIC WAVEFIELD

In 2007, Saudi Aramco initiated an experiment aiming to detect and characterize microseismic energy for reservoir monitoring (Jervis and Dasgupta, 2009). The surface array consisted of 225 buried 3-component stations placed in a 15 by 15 grid with station spacing of 200 m, spanning an area 3 km by 3 km.

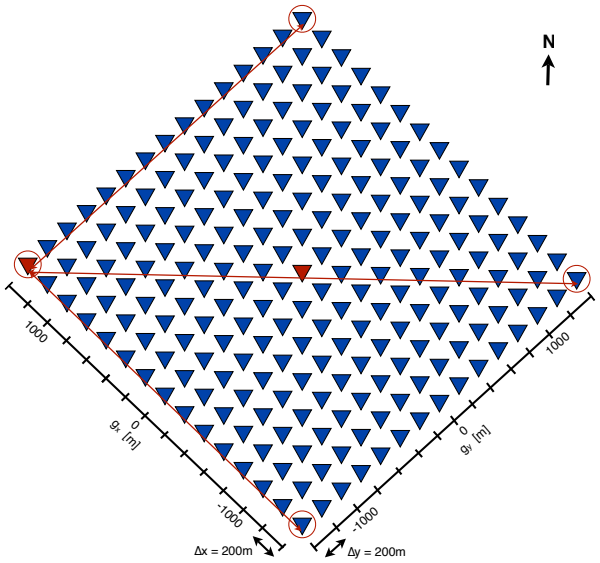

Figure 1: Geometry of the Aramco passive experiment; 225 stations (denoted by triangles) placed in a 15 by 15 grid. The geographic North is indicated by **N**. Red triangles denote stations turned into virtual sources for Figures 7 and 8. Red lines denote receiver lines for sections shown in Figure 7.

Stanford University received a nearly continuous raw data record spanning 48 hours divided over 3 days, starting on day 1 at 18:00 ending on day 3 at 18:00. Only vertical components were used, after removing the arithmetic mean over 30 s time windows. The 48 hours of passive data were analyzed for their spectral characteristics. A frequency domain amplitude spectrogram averaged over the entire array is shown in Figure

2. Most energy was recorded between 2 Hz and 12 Hz and varies in a daily pattern with higher energy during the daylight hours and less energy at night. Figure 3 shows the frequency-domain amplitude spectrum, averaged for all recordings during the hour from 20:00 to 21:00 on day 1, drawn in blue. We identify a peak at very low frequencies, below 1 Hz.

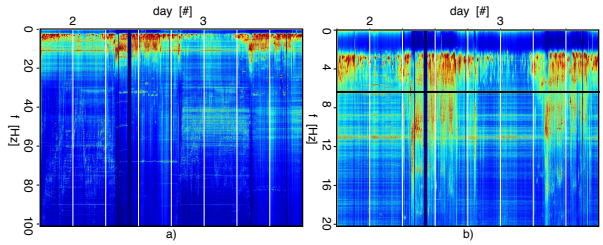

Figure 2: Frequency-domain amplitude spectrum averaged over the array as a function of time for 48 hours. White grid lines denote 6 hour blocks. a) Frequency-domain amplitude spectrum between 0 Hz and 100 Hz; b) frequency-domain amplitude spectrum between 0 Hz and 20 Hz; the black line denotes the frequency of the low-pass filter applied before interferometry.

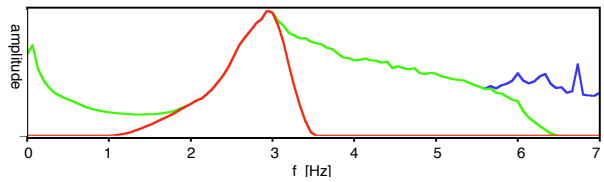

Figure 3: Normalized frequency-domain amplitude spectrum, averaged over the array and data recorded between 20:00 and 21:00 on day 1. The blue curve is the spectrum of the original data record, the red curve is the spectrum of the data after band-pass filtering for beam-forming, and the green line is the spectrum after low-pass filtering for interferometry.

To help determine what kind of seismic energy composes the low-frequency spectrum, the frequency-wavenumber $(f-k_x-k_y)$ domain spectra were computed. A cross section through a cube of frequency-wavenumber spectra averaged over all recordings during the hour from 20:00 to 21:00 on day 1 is shown in Figure 4. The panel in the upper right corner of Figure 4 denotes a beam-forming experiment (see below). A cross section through a cube of frequency-wavenumber spectra averaged over all recordings between 11:00 and 12:00 on day 2 is shown in Figure 5. Both cross-sections only show frequencies below 6 Hz; above 6 Hz no wave modes could clearly be identified. Up to 6 Hz most of the energy resides in the (Rayleigh) surface wave modes. The fundamental mode becomes aliased above 3 Hz. Between 20:00 and 21:00 on day 1 most energy comes from the west, while from 11:00 to 12:00 on day 2 most energy comes from the north. (The directionality of the tails in the frequency-wavenumber spectra is controlled by the sign of the Fourier transformations.) Another common technique to characterize directionality in a wavefield is beam-forming. This was performed, after bandpass filtering between 1 Hz and 3.5 Hz, by computing linear $\tau-p$ transformations over both directions. A beam is formed by averaging the amplitude in the $(\tau-p)$ domain over a certain τ-window. (Note τ denotes the interception times and p denotes the slownesses of the stacking lines of the $\tau-p$ transformation in (t,x) domain). The beams shown in the upper right corners of Figures 4 and 5 show that the fundamental mode travels with a slowness of slightly less than 1 ms/m (corresponding to a velocity of slightly greater than 1000 m/s). A higher mode visible in the frequency-wavenumber domain of Figure 4 can be observed (faintly) to travel with a slowness under 0.4 ms/m (corresponding with a velocity greater than 2500 m/s). Studying averaged frequency-wavenumber domains for other hours shows that the ambient seismic field at frequencies below 6 Hz is generally incident from the west and/or north.

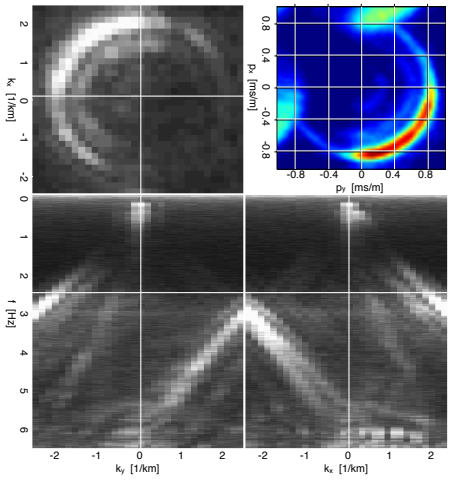

Figure 4: Cross-sections through frequency-wavenumber spectra cube and averaged over the data recorded between 20:00 and 21:00 on day 1. The top right panel contains a beam-forming experiment for the frequency band of 1 Hz to 3.5 Hz.

SOURCES FROM INTERFEROMETRY

Since the coherent ambient seismic field (as recorded by the array) is dominated by surface waves, a low-pass filter of 6.5 Hz was applied to extract the low-frequency surface wave energy. The recordings at all stations are correlated with the recording at one master station, effectively creating a virtual source at that master station. This procedure is repeated using each station as a master station, creating a virtual seismic survey with sources at each station location. The theory of seismic interferometry indicates that the cross-correlation between two recordings should, under equipartitioned energy circumstances, retrieve a time-symmetric Green's function between the stations (Wapenaar, 2004). In Figure 6 the envelope of the Green's functions for a virtual source at $(s_x,s_y)=(0,0)$ m is shown as a series of time slices, computed using all 48 hours of data. The Green's functions are not time-symmetric, which can be expected given the directionality of the ambient seismic

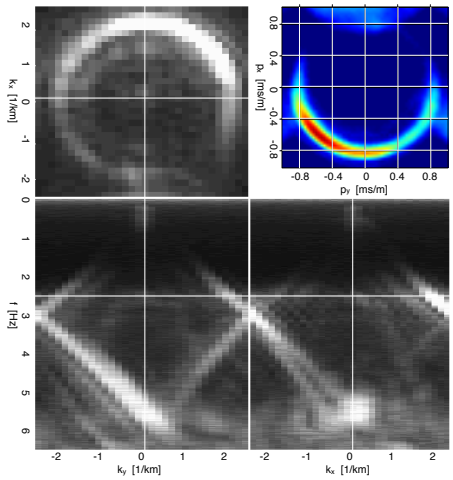

Figure 5: Cross-sections through frequency-wavenumber spectra cube and averaged over the data recorded between 11:00 and 12:00 on day 2. The top right panel contains a beam-forming experiment for the frequency band of 1 Hz to 3.5 Hz.

field at frequencies below 6 Hz. However, the Green's functions are also not symmetric in space. The retrieved Rayleigh wave travels faster through the east than through the west part of the array. The capacity to retrieve longer offsets with less recording is studied by selecting a virtual source at the west end of the array and correlating all recordings between 20:00 and 21:00 on day 1. Figure 7 shows three slices through the correlation cube; a g_x-slice, a g_y-slice and a third diagonal slice (see Figure 1). Although the directionality in the ambient seismic field is favorable for retrieving along the diagonal of the correlation cube, correlating one hour of data was not sufficient to achieve convergence for a Green's function along the long offsets of the diagonal slice. For the smaller offsets along g_x and g_y-slices, one hour of data was sufficient to achieve reasonable convergence. The move-out of the arrivals indicate a velocity of approximately 1000 m/s.

The quality of the retrieved Green's functions depends on the portion of data used and the directionality in the ambient seismic field. To illustrate this, a correlation was computed using each hour of data, for a virtual source at $(s_x, s_y) = (0,0)$ m and stations at the 4 corners of the array. The gathers are shown in Figure 8. The time asymmetry of the retrieved result can be linked to the directionality of the ambient seismic field. For example, for the retrieved signals on day 1 using the data recorded from 20:00 to 21:00, the energy in the correlations is dominantly causal for the station in the south and dominantly acausal for the station in the north, which is consistent with the observation that energy is traveling southwards for this time period. A high concentration of energy arriving at a station focused at approximately $t = \pm 2$ s corresponds to a good convergence rate. The observed convergence rates can be related to the strength of the ambient seismic field (see the frequency spectra of figure 2). Notice the crisp causal Green's functions for daylight hours arriving at the south station.

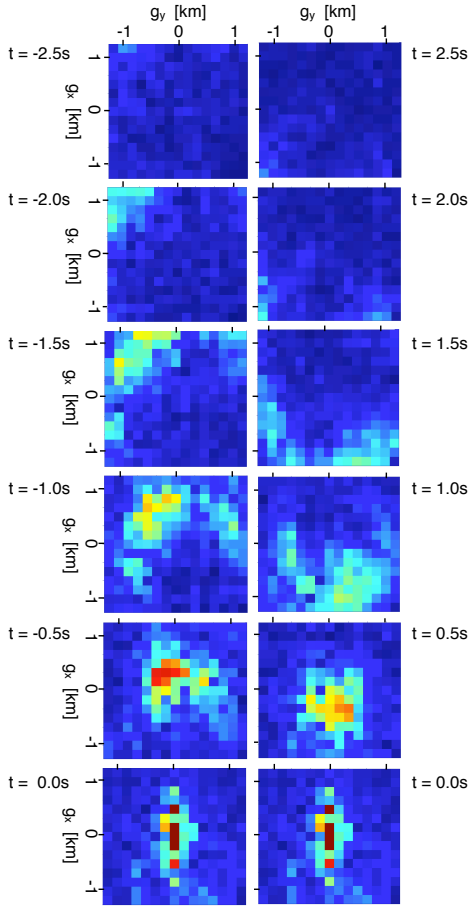

Figure 6: Snap shots of a movie of the acausal (left) and causal (right) parts of retrieved Green's functions for a virtual source at $(s_x, s_y) = (0,0)$ m.

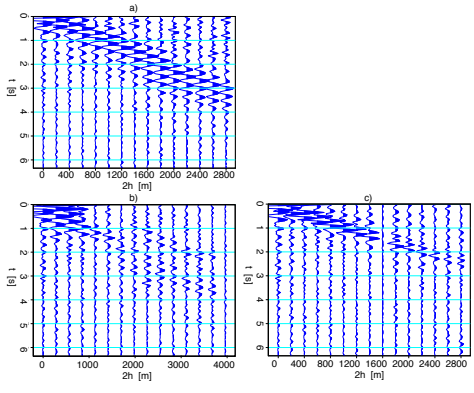

Figure 7: Causal retrieved Green's functions plotted as a function of full offsets (2h) for a source positioned at $(s_x, s_y) = (1400, -1400)$ m. a) A g_x-slice at $g_y = -1400$ m; b) a g_y-slice at $g_x = -1400$ m and; c) a diagonal slice.

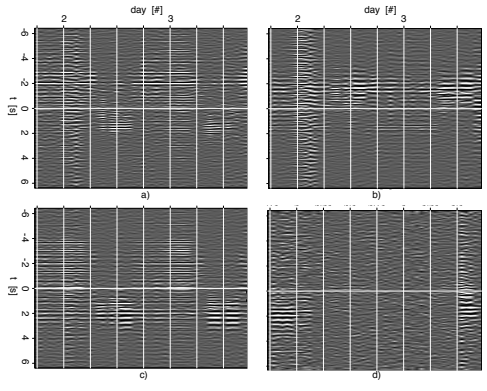

Figure 8: Green's functions for a virtual shot gather of a source positioned at $(s_x, s_y) = (0,0)$ m and stations at; a) $(g_x, g_y) = (1400, -1400)$ m; b) $(g_x, g_y) = (1400, 1400)$ m; c) $(g_x, g_y) = (-1400, -1400)$ m; d) $(g_x, g_y) = (-1400, 1400)$ m.

SPATIAL VARIABILITY AND DISPERSION

Stacking is required to further analyze the obtained virtual seismic survey. First, each spatial axis in the virtual seismic survey is transformed from source-geophone coordinates (s, g), to midpoint (half)offset coordinates (m, h). Then, under a local 1D approximation, the offset coordinates (h_x, h_y) are transformed into cylindrical coordinates and stacked over azimuth. The result is a virtual seismic survey at each midpoint, as a function of radial offset h_r. This result is analogous to the spatial auto-correlation of Aki (1957) (Asten, 2006; Yokoi and Margaryan, 2008). To investigate if there is any spatial variability despite the local 1D approximation, the retrieved Green's function for a full radial offset of $2h_r = 1640$ m are displayed in Figure 9 for two midpoint slices at $m_y = 100$ m and $m_x = 100$ m. Notice the Rayleigh waves arrive earlier for midpoints with negative m_x and positive m_y than for midpoints with positive m_x and negative m_y. This is consistent with the observation of higher velocities on the east side than on that the west end of the array, see previous section. Notice how the dominant phase of the arrival-train travels with a different velocity than the group velocity, indicating dispersion.

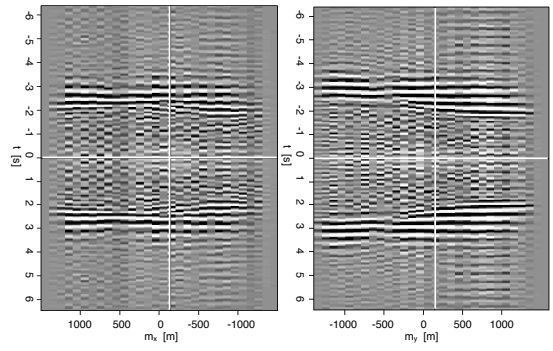

Figure 9: Two slices through a cube of retrieved Green's functions as a function of midpoints, for fixed full radial offset of $2h_r = 1640$ m. Left: $m_y = 100$ m, right: $m_x = 100$ m.

The fundamental mode of a Rayleigh surface wave is represented by a zero-order Bessel function of the first kind, stretched by phase velocity, station distance and frequency (Aki, 1957; Okada, 2003). In Figure 10, this is observed in a frequency range between 1.5 Hz and 6 Hz, for retrieved Rayleigh waves averaged over all midpoints in the array. The jump in the dispersion curve at 4.5 Hz is caused by a poor interpolation technique in the rotation from Cartesian to cylindrical offsets. The lowest retrieved frequencies travel with a wavelength of approximately 1250 m, suggesting sensitivity to a depth of approximately 1250 m. If more data was analyzed, convergence could have been achieved without averaging over azimuth or midpoint, preserving greater detail in subsurface properties for further study, and potentially yielding sufficient energy below 1 Hz and thus sensitivity to greater depth.

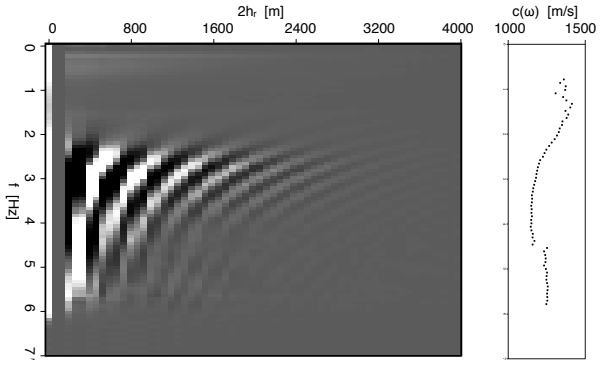

Figure 10: Left; real part of the retrieved Green's functions in the frequency-domain, shown as function of full radial offset, averaged over all midpoints. Right; estimated dispersion curve for the retrieved Green's functions shown in the left panel.

CONCLUSIONS

Rayleigh wave Green's functions were successfully retrieved from 48 hours of ambient seismic noise in the frequency range 1 Hz to 7 Hz. The radiation pattern and convergence rate of the retrieved Green's functions show dependence on the directivity and strength of energy in the ambient seismic field.

ACKNOWLEDGEMENTS

The authors would like to thank Jon Claerbout, Bob Clapp, Jesse Lawrence, Germán Prieto for useful discussions and suggestions. The authors would like to thank the sponsors of the Stanford Exploration Project for their financial support. Special thanks to Saudi Aramco's EXPEC Advanced Research Center for providing data and for permission to publish.

EDITED REFERENCES

Note: This reference list is a copy-edited version of the reference list submitted by the author. Reference lists for the 2010 SEG Technical Program Expanded Abstracts have been copy edited so that references provided with the online metadata for each paper will achieve a high degree of linking to cited sources that appear on the Web.

REFERENCES

Aki, K., 1957, Space and time spectra of stationary stochastic waves, with special reference to microtremors: Bulletin of the Earthquake Research Institute, **35**, 415–456.

Artman, B., 2006, Imaging passive seismic data: Geophysics, **71**, no. 4, SI177–SI187, doi:10.1190/1.2209748.

———, 2007, Passive seismic imaging: PhD thesis, Stanford University.

Asten, M. W., 2006, On bias and noise in passive seismic data from finite circular array data processed using SPAC methods: Geophysics, **71**, no. 6, V153–V162, doi:10.1190/1.2345054.

Bakulin, A., and R. Calvert, 2006, The virtual source method: Theory and case study: Geophysics, **71**, no. 4, SI139–SI150, doi:10.1190/1.2216190.

Berkhout, A. J., and D. J. Verschuur, 2006, Imaging of multiple reflections: Geophysics, **71**, no. 4, SI209–SI220, doi:10.1190/1.2215359.

Bussat, S., and S. Kugler, 2009, Recording noise - estimating shear-wave velocities: Feasibility of offshore ambient- noise surface-wave tomography (ANSWT) on a reservoir scale: SEG Technical Program Expanded Abstracts, **28**, 1627–1631.

Claerbout, J. F., 1968, Synthesis of a layered medium from its acoustic transmission response: Geophysics, **33**, 264–269, doi:10.1190/1.1439927.

Cole, S. P., 1995, Passive seismic and drill-bit experiments using 2-d arrays: PhD thesis, Stanford University.

Dellinger, J., 2008, Low frequencies using conventional sensors: "sign-bit" recording revisited: SEG Technical Program Expanded Abstracts, 27, 149–153.

Dellinger, J. A., and J. Yu, 2009, Low-frequency virtual point-source interferometry using conventional sensors: 71st Meeting, European Associated of Geoscientists and Engineers, Expanded Abstracts, Expanded Abstracts, X047.

Dragonov, D., K. Wapenaar, W. Mulder, J. Singer, and A. Verdel, 2007, Retrieval of reflections from seismic background-noise measurements: Geophys. Res. Let., 34, L04305–1 – L04305–4.

Fu, Q., and Y. Luo, 2009, Locating micro-seismic epicenters in common arrival time domain: SEG Technical Program Expanded Abstracts, **28**, 1647–1651.

Jervis, M., and S. N. Dasgupta, 2009, Recent microseismic monitoring results from VSP and permanent sensor deployments in Saudi Arabia: EAGE Workshop on Passive Seismic, Expanded Abstracts, A10.

Landes, M., N. M. Shapiro, S. Singh, and R. Johnston, 2009, Studying shallow seafloor structure based on correlations of continuous seismic records: SEG Technical Program Expanded Abstracts, 28, 1693–1697.

Okada, H., 2003, The microtremor survey method: Society of Exploration Geophysicists: Geophysical Monograph, No. 12.

Schuster, G. T., J. Yu, J. Sheng, and J. Rickett, 2004, Interferometric/daylight seismic imaging: Geophysical Journal International, **157**, no. 2, 838–852, doi:10.1111/j.1365-246X.2004.02251.x.

Schuster, G. T., and M. Zhou, 2006, A theoretical overview of model-based and correlation based redatuming methods: Geophysics, **71**, no. 4, SI103–SI110, doi:10.1190/1.2208967.

Wapenaar, K., 2004, Retrieving the elastodynamic Green's function of an arbitrary inhomogeneous medium by cross correlation: Phys. Rev. Lett., 93, 254301–1 – 254301–4.

Xiao, X., Y. Luo, Q. Fu, M. Jervis, and S. Dasgupta, and P. Kelamis, 2009, Locate microseismic by seismic interferometry: EAGE Workshop on Passive Seismic, Expanded Abstracts, A22.

Yokoi, T., and S. Margaryan, 2008, Consistency of the spatial autocorrelation method with seismic interferometry and its consequence: Geophysical Prospecting, **56**, no. 3, 435–451, doi:10.1111/j.1365-2478.2008.00709.x.